

# S2Looking: A Satellite Side-Looking Dataset for Building Change Detection

Li Shen

Beijing institution of remote sensing  
Beijing, China  
shenli@bjirs.org.cn

Hao Wei

tianjing university  
Beijing, China  
weihao@tju.edu.cn

jiabao yue

Capital Normal University  
Beijing, China  
yuejiabao2019@cnu.edu.cn

Yao Lu

Beijing institution of remote sensing  
Beijing, China  
yaolu@bjirs.org.cn

Hao Wei

tianjing university  
Beijing, China  
weihao@tju.edu.cn

Rui Chen

tianjing university  
Beijing, China  
ruichen@tju.edu.cn

Hao Chen

BeiHang University  
Beijing, China  
justchenhao@buaa.edu.cn

donghai xie

Capital Normal University  
Beijing, China  
xiedonghai@cnu.edu.cn

Yue Zhang\*

Ao Zhang\*

Shouye Lv\*

Bitao Jiang\*

zhangyue@bjirs.org.cn  
zhanga@bjirs.org.cn  
lvshouye@bjirs.org.cn  
jiangbitao@bjirs.org.cn  
Beijing institution of remote sensing  
Beijing, China

## ABSTRACT

Collecting large-scale annotated satellite imagery datasets is essential for deep-learning-based global building change surveillance. In particular, the scroll imaging mode of optical satellites enables larger observation ranges and shorter revisit periods, facilitating efficient global surveillance. However, the images in recent satellite change detection datasets are mainly captured at near-nadir viewing angles. In this paper, we introduce S2Looking, a building change detection dataset that contains large-scale side-looking satellite images captured at varying off-nadir angles. Our S2Looking dataset consists of 5000 registered bitemporal image pairs (size of  $1024 \times 1024$ ,  $0.5 \sim 0.8$  m/pixel) of rural areas throughout the world and more than 65,920 annotated change instances. We provide two label maps to separately indicate the newly built and demolished building regions for each sample in the dataset. We establish a benchmark task based on this dataset, i.e., identifying the pixel-level building changes in the bi-temporal images. We test several state-of-the-art methods on both the S2Looking dataset and the (near-nadir) LEVIR-CD+ dataset. The experimental results show that recent change detection

methods exhibit much poorer performance on the S2Looking than on LEVIR-CD+. The proposed S2Looking dataset presents three main challenges: 1) large viewing angle changes, 2) large illumination variances and 3) various complex scene characteristics encountered in rural areas. Our proposed dataset may promote the development of algorithms for satellite image change detection and registration under conditions of large off-nadir angles. The dataset is available at <https://github.com/AnonymousForACMMM/>.

## CCS CONCEPTS

• **Applied computing** → **Aerospace; Military**; • **Computing methodologies** → **Matching; Image segmentation**.

## KEYWORDS

datasets, neural networks, change detection, remote sensing

## ACM Reference Format:

Li Shen, Yao Lu, Hao Chen, Hao Wei, Hao Wei, donghai xie, jiabao yue, Rui Chen, Yue Zhang, Ao Zhang, Shouye Lv, and Bitao Jiang. 2018. S2Looking: A Satellite Side-Looking Dataset for Building Change Detection. In *Woodstock '18: ACM Symposium on Neural Gaze Detection, June 03–05, 2018, Woodstock, NY*. ACM, New York, NY, USA, 11 pages. <https://doi.org/10.1145/1122445.1122456>

## 1 INTRODUCTION

Change detection is the process of identifying changes and differences in an object or phenomenon at different times [43]; more

\*All authors contributed equally to this research.

Permission to make digital or hard copies of all or part of this work for personal or classroom use is granted without fee provided that copies are not made or distributed for profit or commercial advantage and that copies bear this notice and the full citation on the first page. Copyrights for components of this work owned by others than ACM must be honored. Abstracting with credit is permitted. To copy otherwise, or republish, to post on servers or to redistribute to lists, requires prior specific permission and/or a fee. Request permissions from [permissions@acm.org](mailto:permissions@acm.org).

Woodstock '18, June 03–05, 2018, Woodstock, NY

© 2018 Association for Computing Machinery.

ACM ISBN 978-1-4503-XXXX-X/18/06...\$15.00

<https://doi.org/10.1145/1122445.1122456>

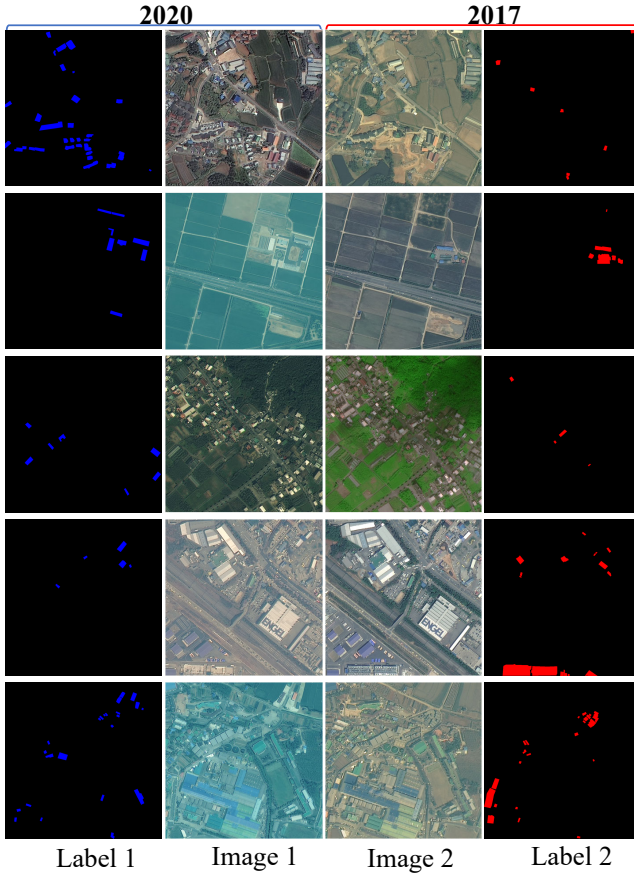


**Figure 1: Samples from the S2Looking dataset. Image 1 and Image 2 are bi-temporal remote sensing images, while Label 1 and Label 2 are the corresponding annotation maps. Label 1 and Label 2 indicate the pixel-precise newly built and demolished building regions respectively. The dataset contains various scenes all over the world, for example village, farm, villa area, retail center and industrial area, which are shown in each row.**

specifically, remote sensing change detection is the process of using multi-temporal remote sensing image data to analyze the same area in order to identify changes in the state information of ground features from the image differences. Remote sensing image change detection plays a crucial role in many fields, such as urban expansion monitoring [24], land use and cover type change monitoring [2, 16], natural disaster monitoring [8], and resource management and evaluation [22].

In recent decades, many change detection methods have been proposed. Depending on the target unit of change, traditional change detection methods include pixel-based methods [19, 45] and object-based methods [25, 32, 55]. Although these traditional methods can be used to extract geometric structural details and set thresholds to obtain detection results, they are easily influenced by variations in image details and quality, which can affect the detection accuracy [46]. In contrast, deep learning, as an important direction of

computer vision research, has undergone remarkable development in recent years [36]. Many scholars have used deep learning methods for remote sensing image processing tasks, such as classification and change detection. Compared with traditional methods, change detection methods based on deep learning, including dual attentive fully convolutional Siamese networks (DASNet) [13], image fusion networks (IFN) [1], end-to-end change detection based on UNet++ (CD-UNet++) [36], fully convolutional Siamese networks based on concatenation and difference (FC-Siam-Conc and FC-Siam-Diff) [15], and a dual-task constrained deep Siamese convolutional network model (DTCDSN) [29], do not require preprocessing to avoid errors to the greatest possible extent [42].

Although deep-learning-based change detection methods outperform other change detection methods in general, the performance of these methods is heavily dependent on the scale, quality and completeness of the datasets used for training the neural networks. Therefore, with the proposal of many change detection methods, a strong demand has emerged for large-scale and high-quality change detection datasets. Some open datasets for remote sensing change detection are available, such as the Change Detection Dataset [53], the WHU Building Dataset [24], the SZTAKI Air Change Benchmark Set (SZTAKI) [4, 5], the OSCD Data Set (OSCD) [15], the Aerial Imagery Change Detection dataset (AICD) [7], and the LEVIR-CD dataset [12] released last year. However, most of these change detection datasets are based on near-nadir imagery captured without scrolling of the mapping satellites or aircraft. The observed building features in these datasets, such as shape, size, and distribution, are relatively simple and cannot be used to comprehensively ensure the performance of a change detection algorithm in practical applications. To a certain extent, this situation limits the development of change detection algorithms.

Compared with near-nadir satellite imagery, side-looking imagery can capture more relevant details of ground objects, and can yield corresponding image information consistent with practical needs. Scroll imaging endows surveillance satellites with a better imaging range and a shorter revisit period than those of mapping satellites [21]. Therefore, the scroll imaging mode at large off-nadir angles can play an important role in the satellite applications, especially in military and disaster rescue contexts. Notably, due to the particular characteristics of side-looking imagery, some of the image detail information may change, which presents a challenge for change detection algorithms. To our knowledge, however, no large-scale side-looking remote sensing image dataset is currently available.

To fill this gap, we introduce a new dataset called S2Looking, short for satellite side-looking rural-area change detection dataset. In terms of scale, both the number of bitemporal image pairs and the number of building change instances are larger than those in than existing datasets. Our new dataset consists of 5000 very high-resolution (VHR) images from the GaoFen (GF), SuperView (SV) and BeiJing-2 (BJ-2) satellites. The imaged areas consist of a number of different globally distributed rural areas, as shown in Figure 1. Notably, due to the characteristics of side-view imaging and complex scenes, the matching of buildings will be relatively difficult. This places higher requirements on an algorithm's robustness when faced with complex ground targets and imaging conditions and increases the practical value of an algorithm that can successfully meet these

challenges. Meanwhile, the S2Looking dataset can also be used to study the fine registration of side-looking remote sensing images.

Overall, our primary contributions are as follows: 1) a pipeline for constructing satellite remote sensing building change detection datasets; 2) a unique large-scale, side-looking, global rural-area remote sensing dataset for building change detection; and 3) a benchmark study generalizing existing algorithms to building update monitoring based on large-scale side-looking images and an outlook on future directions of development for building change detection based on surveillance satellites. We aspire to highlight the challenges faced in the global satellite-based monitoring of building changes, thereby motivating innovation in applications such as battlefield surveillance, natural disaster rescue and monitoring, land allocation, rural floating population research.

## 2 RELATED WORK

In this section, we discuss the related work on change detection in remote sensing images and change detection datasets, which play an important role in the analysis and processing of remote sensing images.

### 2.1 Change detection methods

Deep-learning-based change detection methods can be roughly divided into metric-based methods and classification-based methods. Metric-based methods involve learning an embedding parameter space and calculating the distances between embedded vectors in the space to obtain a change map. Zhan et al. [52] used a deep Siamese fully convolutional network with weight sharing to learn an embedding space and extract features from images captured at different times independently. Sudipan Saha et al. [39] proposed an unsupervised deep change vector analysis method based on a pre-trained convolutional neural network (CNN) and contrastive/triplet loss functions [48, 54]. Chen et al. [13] proposed DASNet to overcome the influence of pseudochange information in the recognition process. Chen et al. [12] proposed a spatial-temporal attention neural network (STANet) based on the FCN-network (STANet-Base) and two improved models with the self-attention modules: basic spatial-temporal attention module (STANet-BAM) and pyramid spatial-temporal attention module (STANet-PAM).

Classification-based methods widely use CNNs to extract the features of bitemporal data and classify the corresponding feature maps. Zhang et al. [1] proposed the IFN model, which relies on a deeply supervised difference discrimination network (DDN) to detect differences in the proposed image features. Peng et al. [36] developed an improved automatic coding structure based on the UNet++ architecture and proposed an end-to-end detection method with a multilateral fusion strategy. Daudt et al. [9, 15] proposed the fully convolutional early fusion (FC-EF) model, which concatenates image pairs before passing them through a UNet-like network, and as well as the FC-Siam-Conc and FC-Siam-Diff models, which concatenate image pairs after passing them through a Siamese network structure. Liu et al. [28] proposed DTCDSCN, in which they introduced spatial attention and channel attention mechanisms to obtain more discriminant features and incorporated semantic segmentation subnetworks for multitask learning. Chen et al. [10] proposed a simple yet effective change detection network (CDNet) which uses

deep siamese fully convolutional networks as the feature extractor and shallow fully convolutional networks as change classifier for the feature difference images. Very recently, Chen et al. [11] proposed an efficient transformer-based model (BiT), which leverages the promising transformer to exploit the global context within token-based space to enhance the image features in pixel space.

### 2.2 Change detection datasets

Large-scale datasets and challenging datasets are critical for training deep-learning-based algorithms. There are many large-scale benchmark datasets available for detection, recognition and segmentation based on everyday images, such as ImageNet [18], COCO [26], PIE [38], MVTec AD [6], Objects365[41], WildDeepfake [56], FineGym [40] and ISIA Food-500 [34]. Large-scale datasets of satellite and aerial imagery are also available. ReID [49] contains 13k vehicle instances captured by unmanned aerial vehicle (UAV) cameras. MOR-UAV [31] consists of 30 UAV videos designed to localize and classify the moving ground objects. WHU [27] consists of thousands of multiview aerial images for the multiview stereo (MVS) matching tasks. DeepGlobe [17] provides three satellite imagery datasets, one for the building detection, one for road extraction and one for land cover classification. xBD [20] and Post-Hurricane [14] consist of post-disaster remote sensing imagery for building damage assessment. SensatUrban [23] contains urban-scale labeled 3D point clouds of three UK cities for fine-grained semantic understanding. FAIR1M [44] provides more than 1 million annotated instances labeled with their membership in 5 categories and 37 subcategories.

In the above datasets, each area is covered by only a single satellite or aerial image. Change detection models need to be trained on datasets consisting of bitemporal image pairs which typically correspond to different sun/satellite angles and different atmospheric conditions. In Table 1, we present the statistics of the existing change detection datasets together with those of our S2Looking dataset. SZ-TAKI [4, 5] contains 13 optical aerial image pairs and considers building changes, the planting of forests, and so on. OSCD [15] focuses on urban regions and includes 24 multispectral satellite image pairs. Different from the other datasets, AICD [7] is a synthetic change detection dataset containing 500 images. The LEVIR-CD dataset [12] consists of 637 manually collected image patch pairs from Google Earth. The Change Detection Dataset [53] is composed of 11 satellite image pairs. The WHU Building Dataset [24] consists of a max-width aerial image collected from a region that suffered an earthquake and was then rebuilt in the following years. In addition to these general change detection datasets, a river change detection dataset [50] has also been released that is specialized for the detection of changes in rivers in hyperspectral images.

The above datasets have greatly promoted the development of change detection methods. However, the images contained in recent satellite change detection datasets have mainly been captured at near-nadir viewing angles. The absence of the large-scale off-nadir satellite image datasets hinders the development of more advanced change detection methods. Thus we introduce the new S2Looking dataset, which is described in more detail in Section 3.

**Table 1: Statistical characteristics of existing change detection datasets**

Dataset	Pairs	Size	Is Real?	Resolution/m	Change Instances	Change Pixels
SZTAKI [4, 5]	12	952×640	✓	1.5	382	412,252
OSCD [15]	24	600×600	✓	10	1,048	148,069
AICD [7]	500	600×800	×	none	500	203,355
LEVIR-CD [12]	637	1024×1024	✓	0.5	31,333	30,913,975
Change Detection Dataset [53]	7/4	4725×2700/ 1900×1000	✓	0.03 to 1	1987/ 145	9,198,562/ 400,279
WHU Building Dataset [24]	1	32507×15354	✓	0.075	2,297	21,352,815
LEVIR-CD+	985	1024×1024	✓	0.5	48,455	47,802,614
S2Looking	5000	1024×1024	✓	0.5~0.8	65,920	69,611,520

### 3 THE S2Looking DATASET

The lacking of public large-scale datasets that cover all kinds of satellites and all kinds of ground surfaces is hindering progress in research on and applications of change detection algorithms. Therefore, by introducing the LEVIR-CD+ and S2Looking datasets, we wish to fill this gap and provide a better benchmark for evaluating change detection algorithms. The LEVIR-CD+ dataset mainly targets urban areas as captured in survey or mapping satellite data from Google Earth. The limitations of the LEVIR-CD+ dataset motivate us to introduce the new S2Looking dataset, which mainly targets rural areas as captured by surveillance or reconnaissance satellites at varying off-nadir angles. The S2Looking dataset represents a more challenging change detection problem. Both datasets are openly available at <https://github.com/AnonymousForACMMM/>.

#### 3.1 Extension of LEVIR-CD+ Dataset

LEVIR-CD+ is based on the LEVIR-CD dataset presented in [12]. Compared with the 637 image patch pairs in the LEVIR-CD dataset released last year, LEVIR-CD+ contains more than 985 VHR (0.5 m/pixel) bitemporal Google Earth images with dimensions of 1024×1024 pixels. These bitemporal images are from 20 different regions located in several cities in the state of Texas in the USA. The capture times of the image data vary from 2002 to 2020. Images of different regions were taken at different times. The bitemporal images have a time span of 5 years.

#### 3.2 Motivation for the New S2Looking Dataset

Different from the LEVIR-CD+ dataset, our new S2Looking dataset mostly targets rural areas throughout the world, imaged at varying large off-nadir angles. Although Google Earth provides free VHR historical images for many locations, Google Earth images are obtained by mapping satellites to ensure high resolution and geometric accuracy. In contrast, side-looking satellite images may offer greater value from the following perspectives: First, optical satellites, especially surveillance satellites, often perform scroll imaging to achieve a better imaging range and a shorter revisit period, as illustrated in Figure 2. For example, when a disaster occurs, scroll imaging by satellites can support analysts in quickly obtaining satellite imagery of the impacted region instead of waiting until a satellite reaches orbit immediately above the region. Additionally, the impacted region

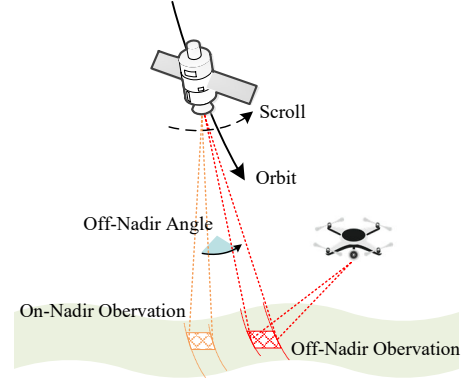


**Figure 2: Illustration of the scroll imaging mode. The satellite scrolls during the imaging process and obtains side-looking remote sensing images.**

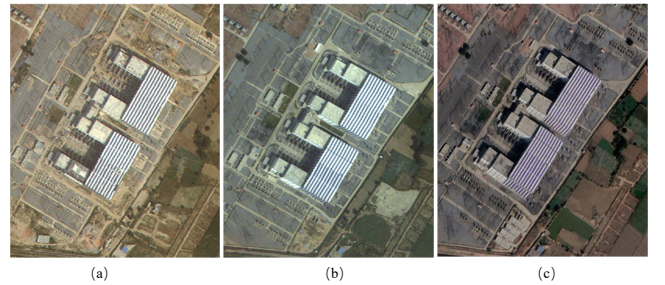


**Figure 3: Examples of side-looking remote sensing images. (a) Near-nadir imagery from Google Earth. (b) Side-looking imagery at an off-nadir angle of 10° from S2Looking. (c) Side-looking imagery at an off-nadir angle of 18° from S2Looking.**

can be more frequently revisited to help anticipate and prevent subsequent disasters. For military applications, scroll imaging by satellites is frequently used to obtain a steady fix on war zones. Second, aerial imagery, including airborne or missile-borne imagery, also tends to be captured at large off-nadir angles to support farther vision given the flight altitude. Because of the similarity between side-looking satellite imagery and aerial imagery, an image processing model designed or trained based on side-looking satellite imagery will also

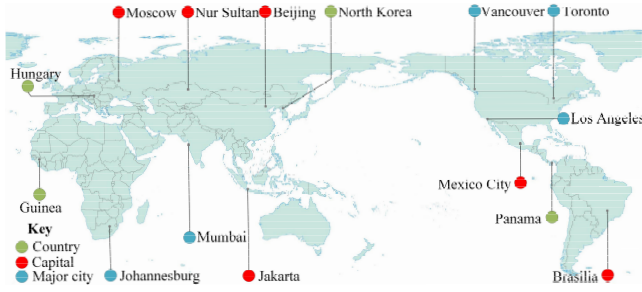


**Figure 4: Locations throughout the world of the bitemporal images represented in the S2Looking dataset.**

be more adaptive to aerial imagery, which makes it applicable for joint operations of satellites and aircraft.

Figure 4 illustrates the geospatial distribution of our new dataset. Most remote sensing images in the S2Looking dataset capture rural areas near the cities marked in Figure 4. For remote sensing change detection, data from rural areas generally have more value than data from urban areas. In regard to military surveillance, sensitive installations are usually built in isolated areas for safety reasons. For disaster rescue in remote regions, satellite images can be obtained faster than aerial photographs because satellites do not have a restricted flying range. Thus, such images are of great value for training remote sensing change detection models that can find and update the status of military installations or destroyed buildings for disaster rescue. For our purposes, we aim to achieve global surveillance for updating building status, which motivates the introduction of the new S2Looking dataset to overcome the limitations of the LEVIR-CD+ dataset.

However, side-looking satellite imagery of rural areas is more difficult to collect than vertical-looking imagery of urban areas. Buildings may be imaged by satellites from different sides and projected along different angles into 2D images, as shown in Figure 3. Table 2 provides a summary of our dataset. The off-nadir angles have an average absolute value of  $9.86^\circ$  and a standard deviation of  $12.197^\circ$ . A frequency histogram of our S2Looking dataset is presented in Figure 5, showing that the off-nadir angles in this dataset range from  $-35^\circ$  to  $40^\circ$ . Thus, it is difficult for a registration algorithm to match feature points between the bitemporal images. Additionally, irrelevant structures such as vegetable greenhouses and small reservoirs can interfere with the building annotation process. An illustration of the data processing pipeline for our S2Looking dataset is shown in Figure 6.

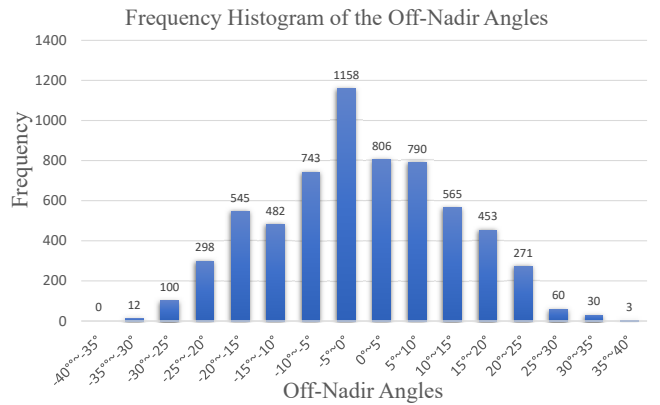
### 3.3 Bitemporal Image Registration

Image registration is essential for the preparation of image pairs for a change detection dataset [51]. Although accurate spatial co-registration for images captured at near-nadir angles can be achieved with accurate digital elevation models (DEMs) [33, 47], the geolocalization accuracy become worse with large off-nadir angles, especially in the case of hilly/mountainous areas [3, 37]. In addition, the dense (with a resolution of 10m) global DEMs are not available for us.

According to our experience, the building change detection task is achievable when the precision of the geometric alignment of

**Table 2: A summary of the S2Looking dataset.**

Type	Item	Value
Image Info.	Total Image Pairs	5000
	Image Size	1024×1024
	Image Resolution	0.5~0.8 m
	Time Span	1~3 years
	Modality	RGB image
Off-Nadir Angle Info.	Average Absolute Value	$9.861^\circ$
	Median Absolute Value	$9.00^\circ$
	Max Absolute Value	$35.370^\circ$
	Standard Deviation	$12.197^\circ$
Accuracy Info.	Registration Accuracy	$\geq 8$ pixels
	Annotation Accuracy	$\geq 2$ pixels



**Figure 5: Frequency histogram of the off-nadir angles of the satellite images in the S2Looking dataset.**

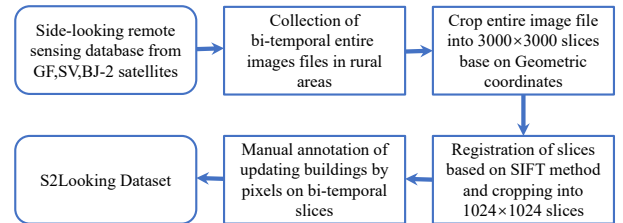


**Figure 6: Data processing pipeline for the S2Looking dataset.**

bitemporal image pairs is less than 8 pixels. Therefore, we use the scale-invariant feature transform (SIFT) algorithm from [30] to find and match feature points in each pair of corresponding images, delete incorrectly matched pairs based on the random sample consensus (RANSAC) homography transformation, and finally resample the images using the homography matrix to achieve alignment between the images, as shown in Figure 7.

The SIFT algorithm constructs a multiscale image space by means of Gaussian filtering and searches for extreme points in the difference of Gaussian (DOG) image as feature points. For feature description,





**Figure 7: Registered feature points. The images in the left and right columns form bitemporal pairs. The numbered points are the matched feature points in the two images.**

the SIFT algorithm uses the gradient direction histogram as the descriptor of the feature points and uses the ratio of the distances to the nearest and second nearest points as the basis for matching. The SIFT algorithm is robust to illumination changes, and can even handle some degree of affine or perspective distortion [35]. To improve the accuracy of the SIFT algorithm, we use the floating-point variable type to store the gray values of each image, thus avoiding missing values due to integer approximation when the Gaussian filtering and DOG results are calculated. To avoid misaligned image pairs and guarantee the registration accuracy, all bitemporal images in the S2Looking dataset have been manually screened by remote sensing image interpretation experts to ensure that the maximum registration deviation is less than 8 pixels. This means that the misaligned area is less than 1/16 of the average building change size in S2Looking (1056 pixels).

Although absolutely accurate registration seems impossible, further improvement of the registration of S2Looking is promising and could improve the performance of change detection models. We hope to see innovative image registration methods and models developed based on the S2Looking dataset.

### 3.4 Annotation Collection and Quality Control

The bitemporal images were annotated by remote sensing image interpretation experts. All newly built and demolished building regions in the dataset were annotated at the pixel level in separate auxiliary graphs, thus making further registration processes possible. The annotation accuracy was required to be higher than 2 pixels. All annotators had rich experience in interpreting remote sensing images and a comprehensive understanding of the change detection task. They followed detailed specifications for annotating the images to yield consistent annotations. Moreover, each sample in our dataset was annotated by one annotator and then double-checked by another to ensure high-quality annotations.

Some selected samples from the dataset are shown in Figure 1. It should be noted that the construction of new buildings and the demolition of old buildings are annotated in separate label images. When further image registration methods are available and the registration accuracy is improved, these label images can be simply adjusted accordingly without the need for any further annotation process.

## 4 CHALLENGE

Buildings are representative man-made structures. During the last few decades, the areas from which our images were collected have seen significant land use changes, especially rural construction, which faces more difficulties than construction in urban areas. Our VHR remote sensing images provide an opportunity for us to analyze subtle changes, such as changes in building instances. Therefore, we focus on building-related changes, including building growth (the change from soil/grass/hardened ground through building construction into newly built-up regions) and building decline. Meanwhile, the relevant applications place high requirements on the accuracy of building change detection.

### 4.1 S2Looking Challenge Statement

The S2Looking dataset was extracted from side-looking rural-area remote sensing images, which makes it an expanded and “hard mode” version of the LEVIR-CD+ dataset. Given training data, the challenge is to create models and methods that can extract building growth and decline polygons quickly and efficiently. Furthermore, these models and methods must assign each polygon to accurately cover the range of building change, meaning that each polygon and building region must be matched pixel by pixel. The evaluation metrics are based on the true positive, false positive, and false negative predicted pixels.

### 4.2 Key Challenges

Many methods have achieved satisfactory results on the LEVIR-CD dataset (F1-score > 0.9) [11, 12], but the performance of these methods on the S2Looking dataset is not sufficient for the use cases of interest, as shown in our experiments in Section 5.2. According to our analysis, the challenges presented by S2Looking compared to LEVIR-CD+ can be summarized as follows.

**Sparse building updates.** The changed building instances in the S2Looking dataset are far sparser than those in the LEVIR-CD+ dataset due to the differences between rural and urban areas. Most rural areas are predominantly covered with farmland and forest, while urban areas are predominantly covered with buildings that are constantly being updated. The average number of change instances in S2Looking is 13.184, while the average number of change instances in LEVIR-CD is 49.188 [12]. This makes it more difficult for networks to extract building features during the training process.

**Side-looking image problem.** The S2Looking dataset concentrates on side-looking remote sensing imagery, which makes the change detection problem different from that on a dataset consisting of Google Earth images. The buildings have been imaged by satellites from different sides and projected along varying off-nadir angles into 2D images, as shown in Figure 3. This phenomenon challenges the ability of a change detection model to identify the same building imaged from different directions and detect the updated parts of the building.

**Complex scenes from rural areas.** Seasonal variations and land cover changes unrelated to building updates are more obvious in rural areas than in urban areas. Farmlands are typically covered by different crops or withered vegetation depending on the season and thus have different appearances in different remote sensing images. A suitable change detection model needs to distinguish building

changes from irrelevant changes in order to generate fewer false positive pixels.

**Registration accuracy problem.** The registration process for the bitemporal remote sensing images in S2Looking is not completely accurate due to the side-looking nature of the images and terrain undulations. Based on manual screening by experts, the registration accuracy of the S2Looking dataset is higher than 8 pixels. This necessitates a change detection model that can tolerate slightly inaccurate registration.

### 4.3 Challenge Restrictions

To better accommodate operational use cases and maintain fairness, the geographic coordinate information has been removed from the data used for inference in the challenge. Thus, no geographic base map database can be applied in the change detection challenge. The models for change detection and subsequent image registration are allowed to extract information only from the images themselves.

## 5 BENCHMARKS

In this section, we first introduce the evaluation metrics for the change detection challenges. Then, we report a thorough evaluation of benchmark and state-of-the-art methods conducted on the LEVIR-CD+ dataset and the S2Looking dataset to establish our dataset as a new baseline for change detection. Finally, we analyze the evaluation results to prove the validity and difficulty of our dataset.

### 5.1 Benchmark Setups

**Statistics of the Train/Val/Test Split.** We evaluated the performance of all methods on the LEVIR-CD+ and S2Looking datasets. The LEVIR-CD+ dataset contains 985 image patch pairs, and we designated 65% of the images as the training set and the remaining 35% as the test set. The S2Looking dataset consists of 5000 image patch pairs, which we split into a training set, a validation set and a test set at proportions of 70%, 10%, and 20%, respectively.

**Evaluation Metric.** In remote sensing change detection, the goal is to infer the changed areas between bitemporal images. To this end, we took three-channel multispectral image pairs as the input and output a single-channel prediction map. The Label 1 and Label 2 maps, when combined into one map, form the pixel-precise ground truth label. The performance of a change detection method is reflected in the differences between the prediction maps and ground-truth maps. To evaluate the performance, we used the Precision, Recall, and F1-score as evaluation metrics.

$$\text{Precision} = \frac{TP}{TP + FP}, \quad (1)$$

$$\text{Recall} = \frac{TP}{TP + FN}, \quad (2)$$

$$\text{F1-score} = \frac{2}{\text{Precision}^{-1} + \text{Recall}^{-1}} \quad (3)$$

Here,  $TP$ ,  $FP$ , and  $FN$  correspond to the numbers of true positive, false positive, and false negative predicted pixels for class 0 or 1. Both Precision and Recall have a natural interpretation in terms of the change detection. Recall can be viewed as a measure of effectiveness in identifying the changed regions. Precision is a measure

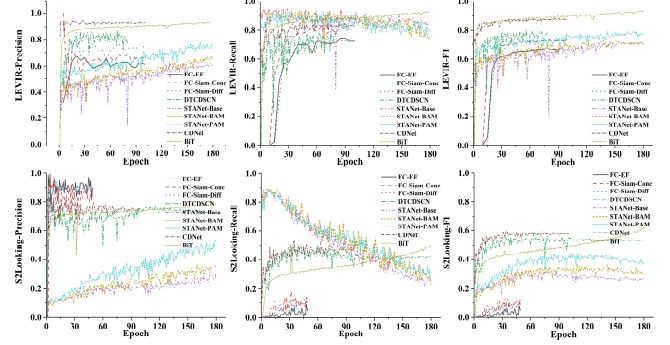


**Figure 8: Results of fine-tuning the algorithms on the LEVIR-CD+ and S2Looking datasets. The top row presents the evaluations of the Precision, Recall and F1-score metrics on the LEVIR-CD+ dataset, and bottom-row represents the evaluations on the S2Looking dataset. Each algorithm took more epochs to converge and obtained lower F1-scores on S2Looking than on LEVIR-CD+.**

**Table 3: Results of the evaluated methods.**

Method	LEVIR-CD+			S2Looking		
	Precision	Recall	F1-score	Precision	Recall	F1-score
FC-EF[15]	0.6130	0.7261	0.6648	0.8136	0.0895	0.0765
FC-Siam-Conc[15]	0.6624	0.8122	0.7297	0.6827	0.1852	0.1354
FC-Siam-Diff[15]	0.7497	0.7204	0.7348	0.8329	0.1576	0.1319
DTCDCN[28]	0.8036	0.7503	0.7760	0.6858	0.4916	0.5727
STANet-Base[12]	0.6214	0.8064	0.7019	0.2575	0.5629	0.3534
STANet-BAM[12]	0.6455	0.8281	0.7253	0.3119	0.5291	0.3924
STANet-PAM[12]	0.7462	0.8454	0.7931	0.3875	0.5649	0.4597
CDNet[10]	0.8896	0.7345	0.8046	0.6748	0.5493	0.6056
BiT[11]	0.8274	0.8285	0.8280	0.7264	0.5385	0.6185

of effectiveness in excluding the irrelevant and unchanged structures from the prediction results. The F1-score provides an overall evaluation of the prediction results; a higher value is better.

**Training Process.** Regarding the implementation details, we followed the settings defined for both the classic and state-of-the-art methods. Due to memory limitations, we kept the original input images with dimensions of  $1024 \times 1024$  for the classic methods (FC-EF, FC-Siam-Conc, FC-Siam-Diff, and DTCDCN) and cropped the images to  $16 \times 256 \times 256$  for the state-of-the-art methods (STANet-Base, STANet-BAM, STANet-PAM, CDNet, and BiT). We trained the detection models on a system with a Tesla P100 GPU accelerator and an RTX 2080 Ti graphics card, and all methods were implemented with PyTorch.

### 5.2 Benchmark Results

We conducted experiments using several remote sensing change detection methods. Figure 8 shows the results of fine-tuning the algorithms on the LEVIR-CD+ and S2Looking datasets. Each algorithm took more epochs to converge and obtained lower F1-scores on S2Looking than on LEVIR-CD+. The evaluation metrics and visualizations of the results of remote sensing change detection for all methods and dataset categories are presented in Table 3 and Figure 9, respectively. The F1-scores of the evaluated methods on the S2Looking dataset are at least 25% less than those on LEVIR-CD+,

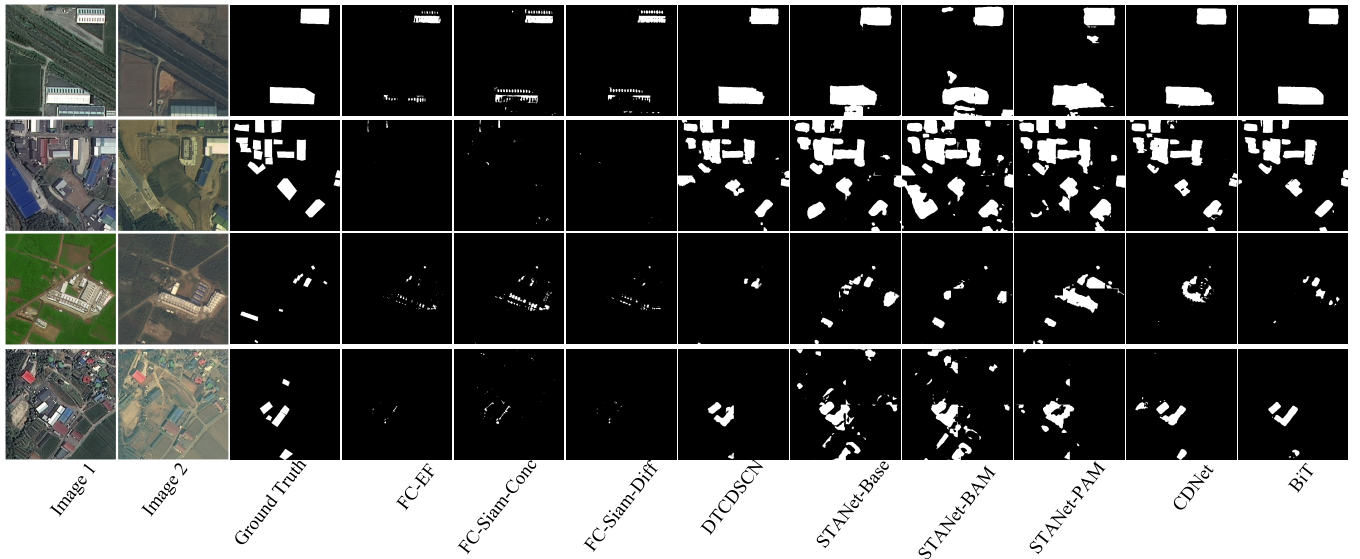


Figure 9: Visualizations of the results of the different methods on the S2Looking dataset.

which shows that S2Looking presents a far more difficult challenge than the other dataset. Consequently, more sophisticated change detection models are needed to efficiently tackle the S2Looking challenge.

The change detection methods evaluated here are basically robust to the seasons and illumination changes in S2Looking, thus making building change detection a solvable problem. We now discuss the overall evaluation results for each method.

**FC-Net** [15] consists of three different models, namely, FC-EF, FC-Siam-Conc, and FC-Siam-Diff. As shown in Table 3, on both datasets, FC-Siam-Conc and FC-Siam-Diff performed better than FC-EF. FC-Net performed poorly on S2Looking compared to its performance on the LEVIR-CD+ dataset. This is because the structure of FC-Net is too simple to be effectively trained on the complex problem presented by the S2Looking dataset. Compared with the DTCDCSCN model, which has 512 channels, the deepest layer of FC-Net has only 128 channels; consequently, the ability of FC-Net to capture feature representations is limited. From the predictions on the test set of the S2Looking, we can observe that the change detection performance of FC-Net is based on image contrast, and this method fails to recognize the building structures. This results in the detection of small objects with strong contrast, such as white cars, darkened windows and the shadows of updated buildings, instead of whole building boundaries as shown in Figure 9.

**DTCDCSCN** [28] is also a Siamese network, but it combines the task of change detection with that of semantic detection. DTCDCSCN contains a change detection module and two semantic segmentation modules. Moreover, it includes an attention module to improve its feature representation capabilities. Compared with FC-Net, DTCDCSCN is more accurate in identifying changed regions and more robust to side-looking effects and building shadows. In addition, DTCDCSCN can better detect small changes in building boundaries in bitemporal images. Therefore, DTCDCSCN performed much better than FC-Net on the S2Looking dataset. However, DTCDCSCN failed to recognize many small prefabricated houses as shown in

the third and fourth rows of Figure 9. Additionally, because of the complex objects presented in rural areas, some large vegetable greenhouses, cultivated lands, hardened ground areas were misrecognized as changed buildings.

**STANet** [12] is a Siamese-based spatial-temporal attention network designed to explore spatial-temporal relationships. The design of STANet includes a base model (STANet-Base) that uses a weight-sharing CNN to extract features and measure the distances between feature maps to detect changed regions. Moreover, STANet includes a basic spatial-temporal attention module (STANet-BAM) and a pyramid spatial-temporal attention module (STANet-PAM) to capture multi-scale spatial-temporal dependencies. As shown in Table 3, STANet-PAM performs better (F1-score) than STANet-BAM and STANet-Base on both datasets. We also find that the STANet tends to have relatively high recall but low precision compared to other methods. It may be because that the batch balanced contrastive loss employed in the training phase gives more weight to the misclassification of the positive samples (change), therefore the model having a tendency to make more positive predictions. Note that STANet-PAM performs better than DTCDCSCN on the LEVIR-CD+ dataset but worse than DTCDCSCN on the S2Looking dataset. We conclude that STANet is more vulnerable to side-looking effects and illumination differences, which are more severe in the S2Looking dataset. Consequently, it became more frequent that sides of building were misrecognized as building changes, which influenced the *FP* value in Equation 1 and thus reduced the Precision.

**CDNet** [10] is a simple yet effective model for building change detection. It consists of a feature extractor (UNet-based deep Siamese fully convolutional networks) to extract image features from a pair of bitemporal patches, and a metric module to calculate bitemporal feature differences, and a relatively simple classifier (a shadow fully convolutional network) to produce change probability maps from the feature difference images. CDNet shows better detection results than the previous methods on both datasets. Due to the effective structure of CDNet, including the deep feature extractor that can well handle



the moderate illumination variances and small registration errors, it may produce high-resolution high-level semantic feature maps. For example, as shown in Fig 9, CDNet is robust in misregistered hilly regions. However, it fails to predict some small prefabricated houses and structures that appeared bright in one bitemporal image and dim in the other were misrecognized as changed buildings. The change discrimination process of CDNet is performed pixel-wisely on the two feature maps, therefore such a model can not handle conditions of big side-looking angles.

**BiT** [11] is an efficient change detection model by leveraging transformers to model global interactions within the bitemporal images. Similar to CDNet, the basic model [11] has a feature extractor and the prediction head. Differently, the BiT model has a unique module (Bitemporal image transformer) to enhance the features. BiT composes of a Siamese semantic tokenizer to generate a compact set of semantic tokens for each bitemporal input, a Transformer encoder to model the context of semantic concepts into token-based space-time, and a Siamese Transformer decoder to project the corresponding semantic tokens back into the pixel space to obtain refined feature maps. Table 3 shows BiT outperforms all the compared methods on the two datasets. In the experimental assessment, only small prefabricated houses on hills were misrecognized due to lower registration accuracy as shown in fourth row of Figure 9. Most incorrect pixel predictions produced by BiT were due to side-looking effects associated with the expansion of building boundaries, which make it more difficult to accurately recognize building boundaries in remote sensing images.

## 6 CONCLUSION

We have introduced the S2Looking dataset, a novel dataset focusing on side-looking remote sensing images of rural areas for building change detection. We have reproduced several classic and state-of-the-art change detection methods on the dataset. To illustrate the difficulty of the proposed S2Looking dataset, we introduced the expanded LEVIR-CD+ dataset for comparison. Experimental results show that contemporary change detection methods perform much less well (25% less on the F1-score) on the S2Looking dataset than on the LEVIR-CD+ dataset. We also gave a throughout analysis of the challenge of the proposed dataset and the weakness of recent change detection pipelines.

We hope our proposed dataset may promote the development of deep-learning-based algorithms for satellite image building change detection and registration under conditions of large off-nadir angles.

## REFERENCES

- [1] Chenxiao Zhang A, Peng Yue B C D, Deodato Tapete E, Liangcun Jiang B, Boyi Shangguan B, Li Huang B, and Guangchao Liu B. 2020. A deeply supervised image fusion network for change detection in high resolution bi-temporal remote sensing images. *ISPRS Journal of Photogrammetry and Remote Sensing* 166 (2020), 183–200.
- [2] Hafez A. Afify. 2011. Evaluation of change detection techniques for monitoring land-cover changes: A case study in new Burg El-Arab area. *World Pumps* 50, 2 (2011), 187–195.
- [3] L. Barazzetti, R. Brumana, B. Cuca, and M. Previtali. 2015. Change detection from very high resolution satellite time series with variable off-nadir angle. *Proceedings of SPIE the International Society for Optical Engineering* (2015).
- [4] C. Benedek and Tamas Sziranyi. 2009. Change Detection in Optical Aerial Images by a Multilayer Conditional Mixed Markov Model. *IEEE Transactions on Geoscience and Remote Sensing* 47, 10 (2009), 3416–3430.
- [5] C. Benedek and T Sziranyi. 2009. A Mixed Markov Model for Change Detection in Aerial Photos with Large Time Differences. In *2008 19th International Conference on Pattern Recognition*.
- [6] P. Bergmann, M. Fauser, D. Sattlegger, and C. Steger. 2020. MVTec AD - A Comprehensive Real-World Dataset for Unsupervised Anomaly Detection. In *2019 IEEE/CVF Conference on Computer Vision and Pattern Recognition (CVPR)*.
- [7] N. Bourdis, BDC Marraud, and H. Sahbi. 2011. Constrained optical flow for aerial image change detection. In *2011 IEEE International Geoscience and Remote Sensing Symposium, IGARSS 2011, Vancouver, BC, Canada, July 24-29, 2011*.
- [8] D. Brunner, G. Lemoine, and L. Bruzzone. 2010. Earthquake Damage Assessment of Buildings Using VHR Optical and SAR Imagery. *IEEE Transactions on Geoscience & Remote Sensing* 48, 5 (2010), 2403–2420.
- [9] R. Caye Daudt, B. Le Saux, and A. Boulch. 2018. Fully Convolutional Siamese Networks for Change Detection. In *2018 25th IEEE International Conference on Image Processing (ICIP)*. 4063–4067. <https://doi.org/10.1109/ICIP.2018.8451652>
- [10] H. Chen, W. Li, and Z. Shi. 2021. Adversarial Instance Augmentation for Building Change Detection in Remote Sensing Images. *IEEE Transactions on Geoscience and Remote Sensing* (2021), 1–16. <https://doi.org/10.1109/TGRS.2021.3066802>
- [11] Hao Chen, Zipeng Qi, and Zhenwei Shi. 2021. Efficient Transformer based Method for Remote Sensing Image Change Detection. [arXiv:2103.00208 \[cs.CV\]](https://arxiv.org/abs/2103.00208)
- [12] H. Chen and Z. Shi. 2020. A Spatial-Temporal Attention-Based Method and a New Dataset for Remote Sensing Image Change Detection. *Remote Sensing* 12, 10 (2020), 1662.
- [13] Jie Chen, Ziyang Yuan, Jian Peng, Li Chen, and Haifeng Li. 2020. DASNet: Dual attentive fully convolutional siamese networks for change detection of high resolution satellite images. *IEEE Journal of Selected Topics in Applied Earth Observations and Remote Sensing* PP, 99 (2020).
- [14] Sean Andrew Chen, Andrew Escay, Christopher Haberland, Tessa Schneider, Valentina Staneva, and Youngjun Choe. 2018. Benchmark Dataset for Automatic Damaged Building Detection from Post-Hurricane Remotely Sensed Imagery. [arXiv:1812.05581 \[cs.CV\]](https://arxiv.org/abs/1812.05581)
- [15] R. C. Daudt, B. Le Saux, A. Boulch, and Y. Gousseau. 2018. Urban Change Detection for Multispectral Earth Observation Using Convolutional Neural Networks. In *IGARSS 2018 - 2018 IEEE International Geoscience and Remote Sensing Symposium*. 2115–2118. <https://doi.org/10.1109/IGARSS.2018.8518015>
- [16] Begüm Demir, Francesca Bovolo, and Lorenzo Bruzzone. 2013. Updating Land-Cover Maps by Classification of Image Time Series: A Novel Change-Detection-Driven Transfer Learning Approach. *IEEE Transactions on Geoscience & Remote Sensing* 51, 1 (2013), 300–312.
- [17] I. Demir, K. Koperski, D. Lindenbaum, G. Pang, J. Huang, S. Basu, F. Hughes, D. Tuia, and R. Raskar. 2018. DeepGlobe 2018: A Challenge to Parse the Earth through Satellite Images. In *2018 IEEE/CVF Conference on Computer Vision and Pattern Recognition Workshops (CVPRW)*. 172–17209. <https://doi.org/10.1109/CVPRW.2018.00031>
- [18] Jia Deng, Wei Dong, R. Socher, Li Jia Li, Kai Li, and Li Fei-Fei. 2009. ImageNet: A large-scale hierarchical image database. *Proc of IEEE Computer Vision & Pattern Recognition* (2009), 248–255.
- [19] David Gómez-Candón, Francisca López-Granados, Juan J. Caballero-Novella, José M. Pea-Barragán, and Luis García-Torres. 2012. Understanding the errors in input prescription maps based on high spatial resolution remote sensing images. *Precision Agriculture* 13, 5 (2012), 581–593.
- [20] Ritwik Gupta, Richard Hosfelt, Sandra Sajev, Nirav Patel, Bryce Goodman, Jigar Doshi, Eric Heim, Howie Choset, and Matthew Gaston. 2019. xBD: A Dataset for Assessing Building Damage from Satellite Imagery. [arXiv:1911.09296 \[cs.CV\]](https://arxiv.org/abs/1911.09296)
- [21] A. F. Habib, E. M. Kim, and C. J. Kim. 2007. New Methodologies for True Orthophoto Generation. *Photogrammetric Engineering & Remote Sensing* 73, 1 (2007), 25–36.
- [22] S. Le Hégarat-Masle, C. Ottlé, and C. Guérin. 2018. Land cover change detection at coarse spatial scales based on iterative estimation and previous state information. *Remote Sensing of Environment* 95, 4 (2018), 464–479.
- [23] Qingyong Hu, Bo Yang, Sheikh Khalid, Wen Xiao, Niki Trigoni, and Andrew Markham. 2021. Towards Semantic Segmentation of Urban-Scale 3D Point Clouds: A Dataset, Benchmarks and Challenges. [arXiv:2009.03137 \[cs.CV\]](https://arxiv.org/abs/2009.03137)
- [24] Shunping Ji, Shiqing Wei, and Meng Lu. 2018. Fully Convolutional Networks for Multisource Building Extraction From an Open Aerial and Satellite Imagery Data Set. *IEEE Transactions on Geoscience and Remote Sensing* 57, 1 (2018), 574–586.
- [25] Tobias Leichte, Christian Gei, Michael Wurm, Tobia Lakes, and Hannes Taubenbeck. 2017. Unsupervised change detection in VHR remote sensing imagery – an object-based clustering approach in a dynamic urban environment. *International Journal of Applied Earth Observation and Geoinformation* 54 (2017), 15–27.
- [26] Tsung Yi Lin, Michael Maire, Serge Belongie, James Hays, and C. Lawrence Zitnick. 2014. Microsoft COCO: Common Objects in Context. (2014).
- [27] Jin Liu and Shunping Ji. 2020. A Novel Recurrent Encoder-Decoder Structure for Large-Scale Multi-View Stereo Reconstruction From an Open Aerial Dataset. In *2020 IEEE/CVF Conference on Computer Vision and Pattern Recognition, CVPR 2020, Seattle, WA, USA, June 13-19, 2020*. IEEE, 6049–6058. <https://doi.org/10.1109/CVPR42600.2020.00609>
- [28] Yi Liu, Chao Pang, Zongqian Zhan, Xiaomeng Zhang, and Xue Yang. 2019. Building Change Detection for Remote Sensing Images Using a Dual Task Constrained Deep Siamese Convolutional Network Model. (2019).
- [29] Yi Liu, Chao Pang, Zongqian Zhan, Xiaomeng Zhang, and Xue Yang. 2020. Building Change Detection for Remote Sensing Images Using a Dual-Task Constrained Deep Siamese Convolutional Network Model. *IEEE Geoscience and Remote Sensing Letters* PP, 99 (2020), 1–5.
- [30] D. G. Lowe. 2004. Distinctive Image Features from Scale-Invariant Keypoints. *International Journal of Computer Vision* 60, 2 (2004), 91–110.
- [31] Murari Mandal, Lav Kush Kumar, and Santosh Kumar Vipparthi. 2020. MOR-UAV: A Benchmark Dataset and Baselines for Moving Object Recognition in UAV Videos (MM '20). Association for Computing Machinery, New York, NY, USA, 2626–2635. <https://doi.org/10.1145/3394171.3413934>
- [32] Masroor, Hussain, Dongmei, Chen, Angela, Cheng, Hui, Wei, David, and Stanley. 2013. Change detection from remotely sensed images: From pixel-based to object-based approaches. *Isprs Journal of Photogrammetry & Remote Sensing* (2013).
- [33] W. Mi, C. Chen, J. Pan, Z. Ying, and X. Chang. 2018. A Relative Radiometric Calibration Method Based on the Histogram of Side-Slither Data for High-Resolution Optical Satellite Imagery. *Remote Sensing* 10, 3 (2018), 381–.
- [34] Weiqing Min, Linhu Liu, Zhiling Wang, Zhengdong Luo, Xiaoming Wei, Xiaolin Wei, and Shuqiang Jiang. 2020. ISIA Food-500: A Dataset for Large-Scale Food Recognition via Stacked Global-Local Attention Network. In *Proceedings of the 28th ACM International Conference on Multimedia (Seattle, WA, USA) (MM '20)*. Association for Computing Machinery, New York, NY, USA, 393–401. <https://doi.org/10.1145/3394171.3414031>
- [35] Luigi Parente, Jim H. Chandler, and Neil Dixon. 2021. Automated Registration of SfM-MVS Multitemporal Datasets Using Terrestrial and Oblique Aerial Images. *The Photogrammetric Record* 36, 173 (2021), 12–35. <https://doi.org/10.1111/phor.12346> <https://onlinelibrary.wiley.com/doi/pdf/10.1111/phor.12346>
- [36] Peng, Zhang, and Guan. 2019. End-to-End Change Detection for High Resolution Satellite Images Using Improved UNet++. *Remote Sensing* 11, 11 (2019), 1382–.
- [37] D. Poli and T. Toutin. 2012. Review of developments in geometric modelling for high resolution satellite pushbroom sensors. *The Photogrammetric Record* 27, 137 (2012), 58–73.
- [38] A. Rasouli, I. Kotseruba, T. Kunic, and J. Tsotsos. 2020. PIE: A Large-Scale Dataset and Models for Pedestrian Intention Estimation and Trajectory Prediction. In *2019 IEEE/CVF International Conference on Computer Vision (ICCV)*.
- [39] Sudipan Saha, Francesca Bovolo, and Lorenzo Bruzzone. 2019. Unsupervised Deep Change Vector Analysis for Multiple-Change Detection in VHR Images. *IEEE Transactions on Geoscience and Remote Sensing* PP, 99 (2019), 1–17.
- [40] D. Shao, Y. Zhao, B. Dai, and D. Lin. 2020. FineGym: A Hierarchical Video Dataset for Fine-grained Action Understanding. *2020 IEEE/CVF Conference on Computer Vision and Pattern Recognition (CVPR)* (2020).
- [41] S. Shao, Z. Li, T. Zhang, C Peng, and J. Sun. 2020. Objects365: A Large-Scale, High-Quality Dataset for Object Detection. In *2019 IEEE/CVF International Conference on Computer Vision (ICCV)*.
- [42] Wenzhong Shi, Min Zhang, Rui Zhang, Shanxiong Chen, and Zhao Zhan. 2020. Change Detection Based on Artificial Intelligence: State-of-the-Art and Challenges. *Remote Sensing* 12, 10 (2020), 1688.
- [43] Ashbindu Singh. 1989. Review Article Digital change detection techniques using remotely-sensed data: International Journal of Remote Sensing: Vol 10, No 6. *International Journal of Remote Sensing* (1989).
- [44] Xian Sun, Peijin Wang, Zhiyuan Yan, Feng Xu, Ruiping Wang, Wenhui Diao, Jin Chen, Jihao Li, Yingchao Feng, Tao Xu, Martin Weinmann, Stefan Hinz, Cheng Wang, and Kun Fu. 2021. FAIRIM: A Benchmark Dataset for Fine-grained Object Recognition in High-Resolution Remote Sensing Imagery. [arXiv:2103.05569 \[cs.CV\]](https://arxiv.org/abs/2103.05569)
- [45] Kun Tan, Xiao Jin, Antonio Plaza, Xuesong Wang, Liang Xiao, and Peijun Du. 2016. Automatic Change Detection in High-Resolution Remote Sensing Images by Using a Multiple Classifier System and Spectral-Spatial Features. *IEEE Journal of Selected Topics in Applied Earth Observations & Remote Sensing* 9, 8 (2016),

- 3439–3451.
- [46] Andrew P. Tewkesbury, Alexis J. Comber, Nicholas J. Tate, Alistair Lamb, and Peter F. Fisher. 2015. A critical synthesis of remotely sensed optical image change detection techniques. *Remote Sensing of Environment* 160 (2015), 1–14.
  - [47] M. Wang, Y. Cheng, Y. Tian, L. He, and Y. Wang. 2018. A New On-Orbit Geometric Self-Calibration Approach for the High-Resolution Geostationary Optical Satellite GaoFen4. *IEEE Journal of Selected Topics in Applied Earth Observations & Remote Sensing* 11, 5 (2018), 1670–1683.
  - [48] Moyang Wang, Kun Tan, Xiuping Jia, Xue Wang, and Yu Chen. 2020. A Deep Siamese Network with Hybrid Convolutional Feature Extraction Module for Change Detection Based on Multi-sensor Remote Sensing Images. *Remote Sensing* 12, 2 (2020), 205–.
  - [49] P. Wang, B. Jiao, L. Yang, Y. Yang, S. Zhang, W. Wei, and Y. Zhang. 2020. Vehicle Re-identification in Aerial Imagery: Dataset and Approach. (2020).
  - [50] Qi Wang, Senior Member, IEEE, Zhenghang Yuan, Qian Du, Fellow, IEEE, Xuelong Li, Fellow, and IEEE. 2019. GETNET: A General End-to-end Two-dimensional CNN Framework for Hyperspectral Image Change Detection. (2019).
  - [51] F. Yamazaki, K. I. Kouchi, M. Kohiyama, N. Muraoka, and M. Matsuoka. 2004. Earthquake damage detection using high-resolution satellite images. In *Geoscience and Remote Sensing Symposium, 2004. IGARSS '04. Proceedings. 2004 IEEE International*.
  - [52] Y. Zhan, K. Fu, M. Yan, X. Sun, H. Wang, and X. Qiu. 2017. Change Detection Based on Deep Siamese Convolutional Network for Optical Aerial Images. *IEEE Geoscience and Remote Sensing Letters* 14, 10 (2017), 1845–1849. <https://doi.org/10.1109/LGRS.2017.2738149>
  - [53] M. Zhang and W. Shi. 2020. A Feature Difference Convolutional Neural Network-Based Change Detection Method. *IEEE Transactions on Geoscience and Remote Sensing* PP, 99 (2020), 1–15.
  - [54] Mengya Zhang, Guangluan Xu, Keming Chen, Menglong Yan, and Xian Sun. 2019. Triplet-Based Semantic Relation Learning for Aerial Remote Sensing Image Change Detection. *IEEE Geoscience and Remote Sensing Letters* (2019).
  - [55] Yongjun Zhang, Daifeng Peng, and Xu Huang. 2017. Object-Based Change Detection for VHR Images Based on Multiscale Uncertainty Analysis. *IEEE Geoscience & Remote Sensing Letters* PP, 99 (2017), 1–5.
  - [56] B. Zi, M. Chang, J. Chen, X. Ma, and Y. Jiang. 2020. WildDeepfake: A Challenging Real-World Dataset for Deepfake Detection. In *MM '20: The 28th ACM International Conference on Multimedia*.